

Chapter 5

Vertical Turbulent Mixing in Atmospheric Models



Song-You Hong, Hyeyum Hailey Shin, Jian-Wen Bao, and Jimmy Dudhia

Abstract This chapter begins by providing a brief historical review of the vertical turbulent mixing schemes, followed by an overall concept of representing vertical turbulent mixing processes in atmospheric models and their classification. Then, the evolutionary features of the so-called Yonsei—University (YSU) scheme are described from the 1990s to the present, focusing on its development strategy for atmospheric phenomena from the planetary scale to the sub-kilometer scale. Limitations in existing schemes and directions for future refinements are given. A comprehensive description of the concept for various vertical turbulent mixing schemes is available in (Stensrud in *Parameterization schemes: keys to understanding numerical weather prediction models*. Cambridge University Press, Cambridge, 2007).

Keywords Turbulent mixing · Planetary boundary layer (PBL) · YSU scheme · Gray-zone PBL · Physical parameterization

5.1 Historical Overview

The earliest generation of atmospheric models had so-called bulk planetary boundary-layer (PBL) schemes and poor vertical resolutions, with only one or two levels in the lowest kilometer. Simple bulk formulas related the lowest levels to

S.-Y. Hong (✉)

University of Colorado/CIRES and NOAA/ESRL/PSL, Boulder, CO, USA

e-mail: songyou.hong@noaa.gov

H. H. Shin · J. Dudhia

NCAR, Boulder, CO, USA

e-mail: hshin@ucar.edu

J. Dudhia

e-mail: dudhia@ucar.edu

J.-W. Bao

NOAA/ESRL/PSL, Boulder, CO, USA

e-mail: Jian-wen.bao@noaa.gov

surface fluxes via the bulk Richardson number. Later as the surface layer became resolvable with a thin ~ 100 -m model layer, similarity theory became relevant, and much observation work in that area could be leveraged to give more physically based surface fluxes of heat and momentum. Current PBL schemes are mostly based on similarity assumptions to connect the lowest layer to the surface.

In the 1970s and 1980s, turbulence modeling increasingly turned to so-called higher-order closure, inspired by the seminal paper on the hierarchy of turbulence closures by Mellor and Yamada (1974). Computational power was increasing rapidly in the 1970s, so there was a general belief that the number of prognostic equations for turbulence statistics could be increased, thereby pushing uncertain closure assumptions to second-order [e.g., turbulence kinetic energy (TKE)] and/or even higher moments, where they would either be simplified or at least not be so critical. For example, such a scheme was adopted for the regional Eta model at the US National Meteorological Center (NMC) [currently, National Centers for Environmental Prediction (NCEP)] (Janjić 1990) based on the ideas of Mellor and Yamada (1982). Together with a diagnosed vertical turbulence length scale, TKE can be used to compute the vertical diffusion coefficients or vertical eddy diffusivities, K . A prognostic TKE approach can be applied to the whole atmospheric column, handling elevated turbulence in the free atmosphere (FA) as well as the atmospheric boundary-layer (ABL) turbulence, while maintaining a memory of the turbulence even after surface forcing ceases. Another trend in the 1990s among the K -diffusion (or eddy diffusivity) schemes was the increasing use of enhanced K -profile methods (similar to O'Brien 1970) along with a nonlocal or countergradient term in the vertical heat transport (similar to Deardorff 1972). The ideas of Troen and Mahrt (1986) helped to quantify these terms as a function of surface heat flux, surface layer stability, and an ABL depth defined in terms of a bulk Richardson number. Holtslag and Boville (1993) applied this approach to replace the local K -diffusion scheme in the US National Center for Atmospheric Research (NCAR) Community Climate Model, second version (CCM2). Hong and Pan (1996) similarly replaced a local K -diffusion scheme in the US NCEP global numerical weather prediction (NWP) model, Medium-Range Forecast (MRF), with one that includes a countergradient term and enhanced K -profile. Another form of nonlocal mixing following the ideas of Blackadar (1979) was adopted by Zhang and Anthes (1982) in their high-resolution PBL used in the Penn State Mesoscale Model 4th Generation (MM4) model. This method persists in the asymmetric convection model (ACM) of Pleim (2007) and includes an entrainment layer. This effort can be regarded as an early precursor to mass-flux approaches by directly mixing the surface layer with higher PBL levels due to subgrid thermals to and from the surface layer.

In the 2000s, the eddy-diffusivity mass-flux (EDMF) approach started to be used in NWP models. This method combines local methods for vertical diffusion, either TKE-based or diagnostic- K -based, with a mass-flux treatment of convective ABL (CBL) thermals using a one-dimensional plume model with a nonlocal mass flux between the surface and the thermal top (Soares et al. 2004). The European Centre for Medium-Range Weather Forecasts (ECMWF) model switched the vertical turbulent

mixing scheme in their operational NW model from a local-K scheme to a cubic K-profile scheme, similar to those mentioned earlier with enhanced values in the middle of the ABL (e.g., Troen and Mahrt 1986; Holtslag and Boville 1993; Hong and Pan 1996), plus a separate mass-flux term represented by an entraining and detraining plume transporting the surface air upward (Siebesma et al. 2007). Following a related but different approach, the US NCAR Community Atmosphere Model version 4 (CAM4) adopted Bretherton and Park's (2009) CAM University of Washington (UW) ABL scheme, which included a diagnostic TKE and a generalized vertical turbulence term with the use of moist-conserved variables (i.e., total specific humidity and liquid-ice static energy) that allow deeper moist and dry layers to mix. The CAM4 physics also separately considers vertical turbulence mixing in shallow clouds (Park and Bretherton 2009) and includes top-down mixing. Since 2000, the YSU ABL scheme (Hong et al. 2006), commonly used in the Weather Research and Forecasting (WRF) model simulations, added explicit entrainment to the medium-range forecast (MRF) ABL countergradient scheme modifying the K-profile to stop at the top of the neutral layer and adding a term proportional to surface buoyancy flux in an entrainment layer above. Meanwhile, the National Oceanic and Atmospheric Administration (NOAA)'s operational regional NWP models—i.e., rapid refresh models [RAP, High-Resolution Rapid Refresh (HRRR)]—switched to another Mellor–Yamada-based TKE scheme with more sophisticated length scales (Nakanishi and Niino 2006). Since 2010, the YSU ABL scheme was further developed to include a top-down enhanced mixing profile driven by radiative cooling at the cloud top (Wilson and Fovell 2018); the NOAA's RAP and HRRR models have been enhancing their Nakanishi–Niino TKE scheme to include an EDMF nonlocal part and shallow convection (Olson et al. 2019). The NCEP Global Forecast System (GFS) (formerly MRF) ABL scheme has replaced their nonlocal turbulence mixing from a purely countergradient term to a hybrid countergradient and mass-flux terms based on the ABL instability (Han et al. 2016).

At present, mesoscale numerical models at high resolutions (i.e., horizontal grid spacing on the order of a few kilometers) produce realistic but only partially resolved convective rolls and cells in the ABL to make up for the “lost” transport if no subgrid scale turbulent mixing scheme is used. Properly representing the vertical turbulence mixing processes in the ABL in a model grid mesh with horizontal spacings in the ABL–LES “gray zone” or Wyngaard's (2004) “Terra Incognita”—where the turbulence in the ABL is partially resolved (e.g., sub-kilometer-scale horizontal spacing for CBL)—remains an active area of research, and several investigators are using LES (e.g., Honnert et al. 2011, 2016; Beare 2014; Shin and Hong 2013, 2015; Shin and Dudhia 2016; Zhou et al. 2017, 2018). Further details in the review of ABL schemes are given in LeMone et al. (2020, AMS, monograph).

5.2 Concept and Classification

Consider a prognostic water vapor (q) equation in Eq. (5.1). The local change of q can be written as

$$\frac{\partial \rho q}{\partial t} = -\frac{\partial \rho u q}{\partial x} - \frac{\partial \rho v q}{\partial y} - \frac{\partial \rho w q}{\partial z} + \rho E - \rho C, \quad (5.1)$$

where ρ is the density of air, u , v , and w are the wind components in x -, y -, and z -directions in the Cartesian coordinates. E and C stand for evaporation and condensation due to diabatic processes, respectively.

In atmospheric models, a value at a specific location can be represented by the sum of grid-mean and subgrid-scale (SGS) perturbation, for example, $u = \bar{u} + u'$, and $q = \bar{q} + q'$ (Fig. 5.1). Here, it is important to note that the model predicts \bar{u} and \bar{q} , and the major issue lies in the fact that how to represent the second-order terms that consists of u' and q' in terms of the first-order mean variables, \bar{u} and \bar{q} . A standard approach to obtain the SGS properties is to utilize the so-called, Reynolds averaging.

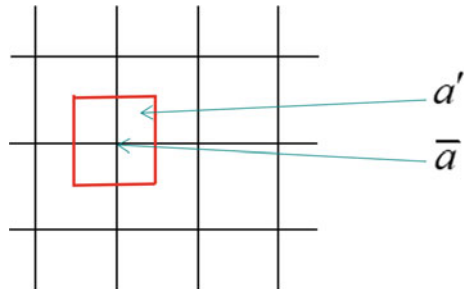
By applying the rule of the Reynolds average, such as $\overline{q'} = 0$, $\overline{u'q'} = 0$, $\overline{\bar{u}q'} = \bar{u}\bar{q}$, Eq. (5.1) can be written as

$$\frac{\partial \rho \bar{q}}{\partial t} = \underbrace{-\frac{\partial \rho \bar{u} \bar{q}}{\partial x} - \frac{\partial \rho \bar{v} \bar{q}}{\partial y} - \frac{\partial \rho \bar{w} \bar{q}}{\partial z}}_{\textcircled{1}} - \underbrace{\frac{\partial \rho \bar{u} q'}{\partial x} - \frac{\partial \rho \bar{v} q'}{\partial y} - \frac{\partial \rho \bar{w} q'}{\partial z}}_{\textcircled{2}} + \rho E - \rho C \quad (5.2)$$

In Eq. (5.2), the grid-resolvable advection, denoted as ①, is represented by model dynamics processes, and the last two terms by moist processes. The remaining issue is how to represent the SGS or turbulent scale processes in ②. By assuming the horizontal homogeneity in the ABL—i.e., $\partial/\partial z \gg \partial/\partial x$ and $\partial/\partial z \gg \partial/\partial y$ —the turbulent term in the vertical direction, $\frac{\partial \rho \bar{w} q'}{\partial z}$, becomes the major SGS contribution to the moisture transport.

In the zeroth-order closure scheme, the effect of turbulent transport, $\frac{\partial \rho \bar{w} q'}{\partial z}$, can be neglected as

Fig. 5.1 Schematic of grid-mean (\bar{a}) and subgrid-scale (SGS) perturbation (a') properties over the model grid. The red box indicates the area of a prognostic variable at a grid point in atmospheric models



$$-\overline{\rho w'q'} = \text{constant}, \quad (5.3)$$

A more physically based representation includes the vertical turbulent flux is proportional to the vertical gradient of grid-mean values, which can be written as

$$-\overline{\rho w'q'} = K \frac{\partial \bar{q}}{\partial z}. \quad (5.4)$$

This formula includes the proportionality function, K , vertical diffusivity (or exchange coefficient), leading to the first-order closure: i.e., parameterizing the second-order moments on the left-hand side (lhs) using the first- and zero-order moments on the right-hand side (rhs).

The next complex level is to predict the turbulent flux as in Eq. (5.1), $\frac{\partial \rho w q}{\partial t} = -\frac{\partial \rho u w q}{\partial x} + \dots$. Then, as in Eq. (5.2), the application of Reynolds averaging leads to the relationship, $\frac{\partial \overline{\rho w'q'}}{\partial t} = \frac{\partial \overline{\rho w'w'q'}}{\partial z}$. Consequently, the rhs term can be written

$$-\overline{\rho w'w'q'} = K' \frac{\partial \overline{\rho w'q'}}{\partial z}, \quad (5.5)$$

where K' is the exchange coefficient resulting from the second-order closure and parameterizing the third-order moments on the lhs using the second- or lower-order moments on the rhs. With this hierarchy of the approximations, the degree of complexity in parameterizing turbulent transport can be classified. The seminar article by Mellor and Yamada (1974) provides the details on the derivation of turbulent kinetic equations.

In a well-mixed layer in the daytime, multiscale turbulent eddies coexist. Vertical velocities within thermals can reach 5 m s^{-1} , although values of $1\text{--}2 \text{ m s}^{-1}$ are more common (Stull 1988). Larger eddies with coherent updrafts are regarded to transport atmospheric properties throughout the ABL (i.e., nonlocal plumes), whereas smaller eddies are regarded to mix the atmospheric properties locally, and their formulations can be expressed as

$$\overline{w'c'} = F_{wc}^L + F_{wc}^{NL} \quad (5.6)$$

and its schematic is given in Fig. 5.2. In Eq. (5.6), c refers to model prognostic variables: e.g., u , v , θ , and q , which refer to zonal and meridional wind components, potential temperature and moisture, respectively: The first term on the rhs describes the local (L) transport by small eddies, whereas the second term for the nonlocal (NL) transport by large eddies. In Fig. 5.2, the surface layer is characterized by a superadiabatic lapse rate, while the entrainment zone on top is stably stratified. z_i is the mixed layer depth that is diagnosed as the vertical level of the minimum heat flux. Given the vertical profiles of potential temperatures and heat flux, one can tell that the upper part of the mixed layer is slightly stable, whereas it is unstable in its below. This indicates a countergradient mixing in the upper part of the mixed layer since

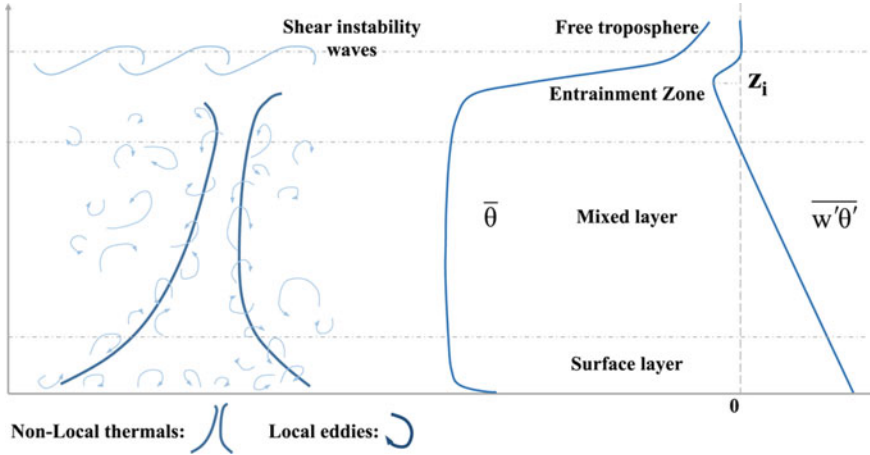


Fig. 5.2 (left) Schematic of the nonlocal thermals and local eddies, as well as (right) the potential temperature and heat flux profiles of the convective boundary layer. From Zhou et al. (2018). ©American Geophysical Union. Used with permission

upward heat flux appears in thermally stabilized layers. This locally countergradient fluxes are associated with nonlocal thermals that span the depth of the mixed layer (left of Fig. 5.2). The nonlocal term can be parameterized as a mass-flux term or a countergradient gamma term (γ_c) which is an addition to the local transport. More details on NL transport term is provided in Sect. 2.2.

The vertical turbulence mixing scheme can be classified as a local versus nonlocal diffusion approach and further by the following 4 categories.

5.2.1 Local Diffusion (Louis 1979)

The local diffusion scheme, the so-called local- K approach (Louis 1979),

$$\frac{\partial c}{\partial t} = \frac{\partial}{\partial z}(-\overline{w'c'}) = \frac{\partial}{\partial z} \left(k_c \frac{\partial c}{\partial z} \right), \tag{5.7}$$

had been utilized for the entire atmosphere at NCEP GFS prior to the MRF PBL. In this scheme, the vertical diffusivity coefficients for momentum and mass (u, v, θ, q) are represented by

$$K_{m,t} = l^2 f_{m,t}(\text{Rig}) \left| \frac{\partial U}{\partial z} \right| \tag{5.8}$$

in terms of the mixing length (l), the stability functions ($f_{m,t}(\text{Rig})$), and the vertical wind shear ($|\frac{\partial U}{\partial z}|$, where U is the horizontal wind speed).

The stability functions, $f_{m,t}$, are represented in terms of the local gradient Richardson number

($\text{Rig} = g/T \left(\frac{\partial\theta_v/\partial z}{|\partial U/\partial z|^2} \right)$, where g is the gravitational constant and θ_v is the virtual potential temperature) at a given level. The mixing length scale, l , is given by

$$\frac{1}{l} = \frac{1}{kz} + \frac{1}{\lambda_0}, \quad (5.9)$$

where k is the von Karman constant (≈ 0.4), z is the height from the surface, and λ_0 is the asymptotic length scale. λ_0 can be a constant or a function of vertical grid spacing as in WRF.

5.2.2 Nonlocal Diffusion with Countergradient Term (Troen and Mahrt 1986)

According to Deardorff (1972), Troen and Mahrt (1986), and Hong and Pan (1996), the turbulence diffusion equations for prognostic variables (c ; u , v , θ , q) can be expressed by

$$\frac{\partial c}{\partial t} = \frac{\partial}{\partial z} (-\overline{w'c'}) = \frac{\partial}{\partial z} \left[K_c \left(\frac{\partial c}{\partial z} - \gamma_c \right) \right], \quad (5.10)$$

where K_c is the eddy-diffusivity coefficient and γ_c is a correction to the local gradient which incorporates the contribution of the large-scale eddies to the total flux. This correction applies to θ and q in Troen and Mahrt (1986) and Hong and Pan (1996) within the mixed boundary layer.

In the daytime mixed layer, the momentum diffusivity is formulated as

$$K_{zm} = kw_s z \left(1 - \frac{z}{h}\right)^p, \quad (5.11)$$

where p is the profile shape exponent taken to be 2. h is the height of the PBL. The mixed layer velocity scale is represented as

$$w_s = u_* \phi_m^{-1}, \quad (5.12)$$

where u_* is the surface frictional velocity scale, and ϕ_m is the wind profile function evaluated at the top of the surface layer. The countergradient terms for θ and q are given by

$$\gamma_c = b \frac{\overline{(w'c')}_0}{w_s}, \quad (5.13)$$

where $\overline{(w'c')}_0$ is the corresponding surface flux for θ and q , and b is a coefficient of proportionality. In order to satisfy the compatibility between the surface layer top and the bottom of the PBL, the identical profile functions to those in surface layer physics are used.

The boundary-layer height is given by

$$h = \text{Rib}_{\text{cr}} \frac{\theta_{\text{va}} |U(h)|^2}{g(\theta_v(h) - \theta_s)}, \quad (5.14)$$

where Rib_{cr} is the critical Bulk Richardson number, $U(h)$ is the horizontal wind speed at h , θ_{va} is the virtual potential temperature at the lowest model level. $\theta_v(h)$ is the virtual potential temperature at h , and θ_s is the appropriate temperature near the surface. The virtual potential temperature near the surface is defined as

$$\theta_s = \theta_{\text{va}} + \theta_T \left(= b \frac{\overline{(w'\theta'_v)}_0}{w_s h} \right), \quad (5.15)$$

where θ_T is the scaled virtual potential temperature excess near the surface.

The eddy diffusivity for temperature and moisture ($K_{\text{zt}} = K_{\text{zm}} \text{Pr}^{-1}$) is computed from K_{zm} in (5.11) by using the relationship of the Prandtl number (Pr), which is given by

$$\text{Pr} = \left[\frac{\phi_t}{\phi_m} + bk \frac{0.1h}{h} \right], \quad (5.16)$$

where Pr is a constant within whole mixed boundary layer.

In addition to the inclusion of the nonlocal gamma term in Eq. (5.10), another main ingredient of the Troen and Mahrt concept is the height of ABL, h , which locates the top of entrainment layer by adding thermal excess and by using the critical Ri greater than 0 (Fig. 5.3). Thus, this approach represents the downward mixing in the entrainment layer implicitly by locating h above the minimum flux level.

5.2.3 Nonlocal Diffusion with Eddy Mass-Flux Term (Siebesma et al. 2007)

This approach utilizes a plume model to represent the strong updrafts. Instead of $K_c \gamma_c$ in Eq. (5.10), a mass-flux term, $M(c_u - \bar{c})$, where c_u is c of the strong updrafts, is introduced, and expressed as

$$\frac{\partial c}{\partial t} = \frac{\partial}{\partial z} (-\overline{w'c'}) = -\frac{\partial}{\partial z} \left[-k_c \frac{\partial \bar{c}}{\partial z} + M(c_u - \bar{c}) \right] \quad (5.17)$$

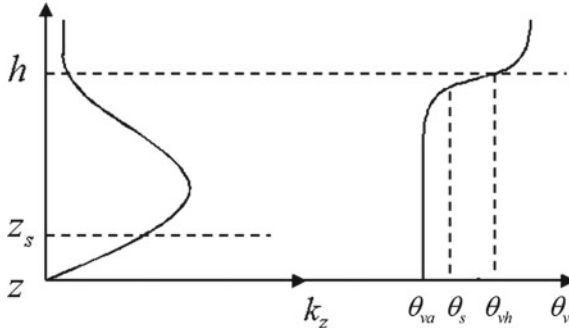


Fig. 5.3 Schematic of the Troen and Mahrt nonlocal scheme. The left panel shows a parabolic shape of diffusion coefficients in Eq. (5.11) with $p = 2$, and the right panel describes the definition of ABL height, h , due to the contribution of the thermal excess in Eq. (5.15) and the Rib_{cr} with 0.5. θ_{vh} is virtual potential temperature at h , and θ_{va} and θ_s are as defined in Eq. (5.11)

The mass-flux, $M = a_u w_u$, where a_u is a fractional area of the strong updrafts in the model grid box under consideration, is directly proportional to w_u since a_u is constant by definition. The updraft velocity w_u can be obtained by

$$\frac{1}{2}(1 - 2\mu) \frac{\partial w_u^2}{\partial z} = -b_u \varepsilon w_u^2 + B, \tag{5.18}$$

where μ and b_u are proportionality factors, ε the fractional entrainment rate, and B the buoyancy term. This approach is an advanced, as compared to the Troen and Mahrt approach, since it utilizes a convective plume model with entrainment and detrainment processes.

By the comparison of the countergradient term in Troen and Mahrt (1986) and the mass-flux term in Siebesma et al. (2007), one can tell that the nonlocal transport term with gamma and mass flux contributes to the total flux in the same way as stabilizing the column (Fig. 5.4). It is also seen that the ED-CG model gives a stable potential temperature profile in the upper half of the boundary layer. In contrast, the ED-MF model reproduces the well-mixed ABL, which is consistent with the LES results. Siebesma et al. (2007) explained that this over-stabilization in the ED-CG approach is due to the countergradient term always being positive, which reduces the top-entrainment flux. Consequently, the BL height of the countergradient experiment is slow compared to the EDMF approach. This behavior of the ED-CG experiment is contradictory to the study of Hong and Pan (1996), with a deeper ABL depth with the countergradient nonlocal mixing over the profile with a local diffusion only. The stabilized profile in the upper part of ABL is an intrinsic nature of the Troen and Mahrt approach, but the behavior of the scheme in specific models depends upon how it is configured.

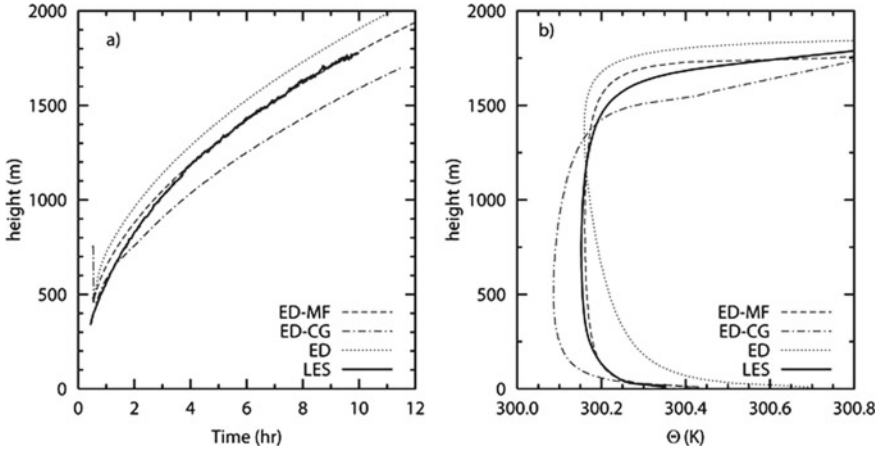


Fig. 5.4 **a** Time evolution of the inversion height for the three different approaches with local diffusion (ED), eddy mass flux (ED-MF), eddy countergradient term (ED-CG) along with LES results as a reference. **b** The mean potential temperature profiles after 10 h of simulation. From (Siebesma et al.2007). ©American Meteorological Society. Used with permission

5.2.4 TKE (Turbulent Kinetic Energy) Diffusion (Mellor and Yamada 1982)

The TKE scheme predicts the turbulent kinetic energy, $u_i u_j$, as a prognostic variable, which can be written as,

$$\frac{\partial \overline{u_i u_j}}{\partial t} + u_j \frac{\partial \overline{u_i u_j}}{\partial x_j} = -\frac{\partial}{\partial x_k} \left[\overline{u_i u_j u_k} + \frac{1}{\rho} \dots \right], \quad (5.19)$$

where i, j , and k denote the vector index to x -, y -, and z -directions in Cartesian coordinates. The expressions for the eddy diffusivities K are complex and include terms related to the environmental wind shear and stability, but can be represented in conceptual form as

$$K_z = L(\overline{u_i u_j})^{1/2}, \quad (5.20)$$

where L is again one of the empirical length scales. It is noted that the lower order TKE scheme, such as the MYJ scheme, is essentially a local mixing concept since the tendency is computed using the local scheme with the K_z diffusivity that was calculated in the TKE equations. The MYNN scheme uses higher-order terms to represent the countergradient term.

5.3 Evolution of a Nonlocal Diffusion Scheme (MRF-YSU-ShinHong-3DTKE Schemes)

This section provides a hierarchy of a nonlocal diffusion scheme since MRF PBL scheme, as summarized in Table 5.1.

5.3.1 Medium-Range Forecast Model (MRF) Scheme

Prior to 1996 at NCEP, there was no explicit planetary boundary layer (PBL) parameterization—diffusivity coefficients were parameterized as functions of the local Richardson number (Eq. (5.1)). Thus, the local- K approach (by Louis 1979) is used for both boundary layer and free atmosphere. This scheme has been widely used because it is computationally inexpensive and produces reasonable results under typical free convection regimes. However, the scheme cannot handle conditions when the atmosphere is well mixed because of the countergradient fluxes; i.e., there is active turbulent mixing in the ABL that occurs against the local gradient of meteorological variables, while Eq. (5.7) computes vertical mixing as 0 when the ABL is well mixed, and therefore, there is no local gradient. Thus, the method is not well-behaved for unstable conditions.

For the above reasons, Hong and Pan (1996) adapted the Troen and Mahrt concept. The strategy is to add the nonlocal features to the Louis-type local scheme and considers the fundamental differences between the local and nonlocal schemes. By examining the impact of parameters in the scheme, the countergradient term is found to be responsible for the well-mixed PBL structure. Other parameters, such as shape parameters, are found to be of a similar impact as described in Troen and Mahrt. θ_T

Table 5.1 Evolution of a nonlocal vertical diffusion scheme

Scheme	Date	Description
MRF	1995	Operational at NCEP GFS model (Hong and Pan 1996)
	1996	Implemented onto Mesoscale Model 5th generation (MM5)
YSU	2004	First implementation in WRF (Hong et al. 2006)
	2008	Enhanced stable layer mixing (Hong 2010)
	2009	Implicit momentum forcing for numerical stability
	2010	Revised w_s computation in stable boundary layer
	2011	Revised thermal excess term (Shin et al. 2012)
	2012	Revised Prandtl number for free convection
	2015	Top-down mixing (Wilson and Fovell 2018)
Shin-Hong	2015	First implementation in WRF (Shin and Hong 2015)
3DTKE	2019	First implementation in WRF (Zhang et al. 2018)

sometimes could become too large when the surface wind is very weak, resulting in unrealistically large h . This large h due to unrealistic θ_T does not harm the results because the diffusivity coefficients are usually very small in these situations, but it is not desirable for diagnostic purposes. For this reason, a maximum limit of θ_T as 3 K is applied.

In implementing the Troen and Mahrt nonlocal concept onto the MRF model, it was found that the determination of the boundary-layer height, h , turns out to be a crucial factor. In the MRF PBL, h is obtained iteratively (see Fig. 5.3). First, h is estimated by Eq. (5.14) without considering the thermal excess, θ_T . This estimated h is utilized to compute the mixed layer velocity, w_s Eq. (5.12). Using w_s and θ_T in Eq. (5.15), h is enhanced. With the enhanced h and w_s , K_{zm} , is obtained by Eq. (5.11), and K_{zt} by Eq. (5.16). The countergradient correction terms for θ and q in Eq. (5.10) are also obtained by Eq. (5.13). In order to avoid the dependency of vertical grid spacings, h is determined by comparing the Rib at a level with the Rib_{cr} by increasing the level from the 2nd model level in its above. h is finalized at the level of Rib = Rib_{cr} by applying a linear interpolation with respect to z .

The main concept of Troen and Mahrt is the addition of nonlocal terms. One can tell that the magnitude of nonlocal mixing is a multiple product, γK . By applying the derivative to Eq. (5.11) with respect to z , one can tell that the maximum value of this quantity locates at $1/3 h$. In the local scheme, the mixed layer should stay unstable in order to transport heat upward, whereas the nonlocal term cools the layer below $1/3 h$ and heats the column in its above, which consequently results in the mixed layer to be neutral or weakly stable in the upper part of the mixed layer.

Unlike a negligible impact of the PBL height that was determined by the critical Ri (Rib_{cr}) for dry conditions (Troen and Mahrt 1986), this parameter is found to play a crucial role in organizing the precipitating convection (Fig. 5.5). The impact of Rib_{cr} on precipitation forecasts was found to be significant on heavy rain case for 15–17 May 1995. Less effective mixing with lower PBL height (due to lower Rib_{cr}) most likely leads to similar precipitation as a local scheme. However, a nonlocal PBL scheme experiment with larger Rib_{cr} (Rib_{cr} = 0.75) shows more effective mixing and gives a boundary-layer structure that is favorable for precipitating convection, leading to more organized precipitation. This behavior is most likely due to the fact that simulated precipitating convection is more sensitive to the boundary-layer structure when the PBL collapses than when it develops. This finding could be generalized if buoyancy-driven local convection typically occurs in the late afternoon or evening.

A scientific milestone of the Hong and Pan study is their finding that efforts to improve the surface and PBL formulation are as important as efforts to improve the precipitation physics in atmospheric models and should be a prerequisite to realizing better precipitation forecasts. The MRF PBL scheme became operational in NCEP in October 1995 and was implemented in the Pennsylvania State University (PSU)/National Center for Atmospheric Research (NCAR) Mesoscale Model 5 (MM5) in 1996.

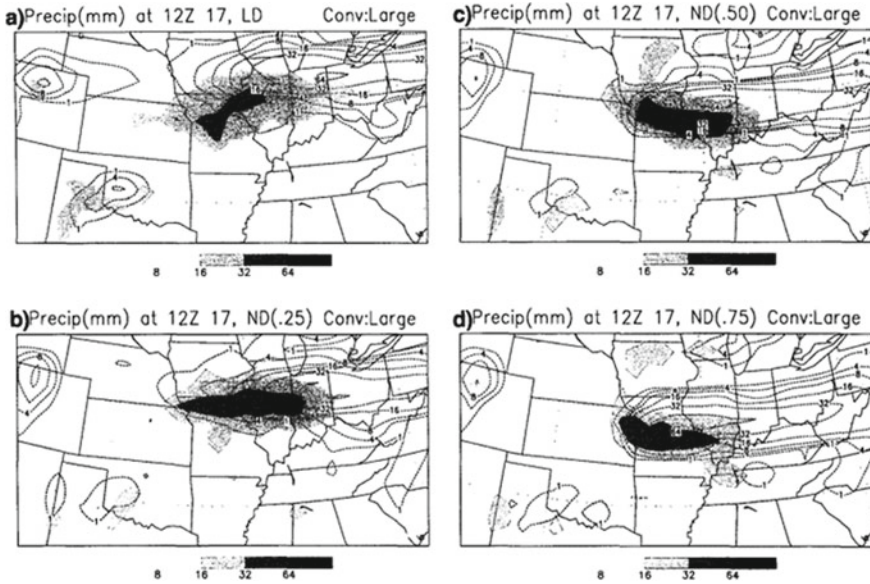


Fig. 5.5 Convective (shaded areas) and large-scale (dotted lines) rainfall (mm) ending at 1200 UTC 17 May 1995 for, **a** the local and nonlocal experiments with, **b** $Rib_{cr} = 0.25$, **c** $Rib_{cr} = 0.50$, and **d** $Rib_{cr} = 0.75$. From Hong and Pan (1996). ©American Meteorological Society. Used with permission

5.3.2 YSU Scheme

In the late 1990s, it was reported that the MRF PBL scheme tended to overmix in general. This behavior was detrimental to the accurate prediction of air pollutants in the Community Multiscale Air Quality Modeling System (CMAQ) when the meteorological input data was obtained from GFS (1999, personal communication with Dr. D. Byun). Also, excessive mixing accompanying too dryness and heating was reported by the evaluation of MM5 forecasts. These behaviors were also known to NCEP, but the scheme remained unchanged since a weakened mixing by reducing the Rib_{cr} in the MRF PBL scheme tends to deteriorate the precipitation forecasts.

It was found that the overall excessive mixing in the MRF PBL is mainly due to the uncertainty in the Troen and Mahrt concept. As seen below, the MRF PBL scheme represents the entrainment of the free tropospheric air into the mixed layer underlying it by locating the ABL height above the minimum flux level. In other words, the entrainment layer is located below h , and the vertical mixing using Eq. (5.10) is applied from the surface to h (see Fig. 5.3). The thermal excess term in Eq. (5.15) can be as large as 2 ~ 3 K in clear-sky conditions, and the corresponding excess due to $Rib_{cr} = 0.5$ can be as large as 3 K when wind speed is 15 m s^{-1} . The resulting thermal excess greater than 5 K tends to locate the PBL height unphysically higher

level (see Fig. 5.3). This behavior is often observed when winds are strong, for example, hurricane predictions.

To overcome inherent deficiencies in the Troen and Mahrt concept, Noh et al. (2003) derived a new formula for entrainment from the LES model. The modifications in Noh et al. (2003) involve three parts. First, the heat flux from the entrainment at the inversion layer is incorporated into the heat and momentum profiles, and it is used to predict the growth of the PBL directly. Second, profiles of the velocity scale and the Prandtl number in the PBL are proposed, in contrast to the constant values used in the TM model. Finally, the nonlocal mixing of momentum was included.

The new PBL model demonstrated the improved predictability of the PBL height and more realistic profiles of potential temperature and velocity as compared to the Troen and Mahrt. They also found that explicit representation of the entrainment rate is the most critical among the three modifications, which is expressed as

$$-\overline{w'\theta'} = K_h \left(\frac{\partial\theta}{\partial z} - \gamma_h \right) \left[\overline{w'\theta'_h} \left(\frac{z}{h} \right)^3 \right] \quad (5.21)$$

The new scheme was found to be promising in LES vertical resolution (about 20 m); however, it is not straightforward to implement it in an NWP model having a coarser vertical resolution (a few 10–100 m with height). For instance, vertical grid spacing ranges 100 ~ 300 m in the PBL in the daytime, a precise estimate of h and is a crucial component. Also, entrainment depth (typically a few 10 m) needs to be accurately represented by the grid-point values of models at coarse vertical resolution. This numerical discretization took more than a year. After early release of the YSU scheme in 2003, about three years were taken to adjust the package to be balanced with other part of physical processes (Fig. 5.6). The paper of Hong et al. (2006) on the final version of the YSU scheme was submitted in early 2006.

In the early version of YSU PBL, the characteristic behavior over the MRF PBL was clearly demonstrated in the clear-sky turbulence region (Fig. 5.7). A typical sounding from Tennessee shows a significant difference in the PBL depth in this case. Overall cooling and moistening of YSU over MRF indicate the accurate representation of the entrainment processes in Noh et al. (2003). This difference is more exaggerated here than in most other situations, but it shows that the shallower moister PBL produced by the YSU scheme has more CAPE than the deeper and drier PBL produced by the MRF scheme.

A major challenge that the early version of the YSU scheme faced lies in the fact that the scheme tends to produce spurious light precipitation and less-organized strong convection. By refining some aspects of the formulation, for example, entrainment fluxes, the scheme showed an overall improvement in precipitation forecasts.

A large region of significantly higher CAPE in Fig. 5.7 is due to the reduced entrainment of dry air into the PBL during the morning hours, which is a direct result of the entrainment parameterization of the YSU PBL, as seen from the idealized

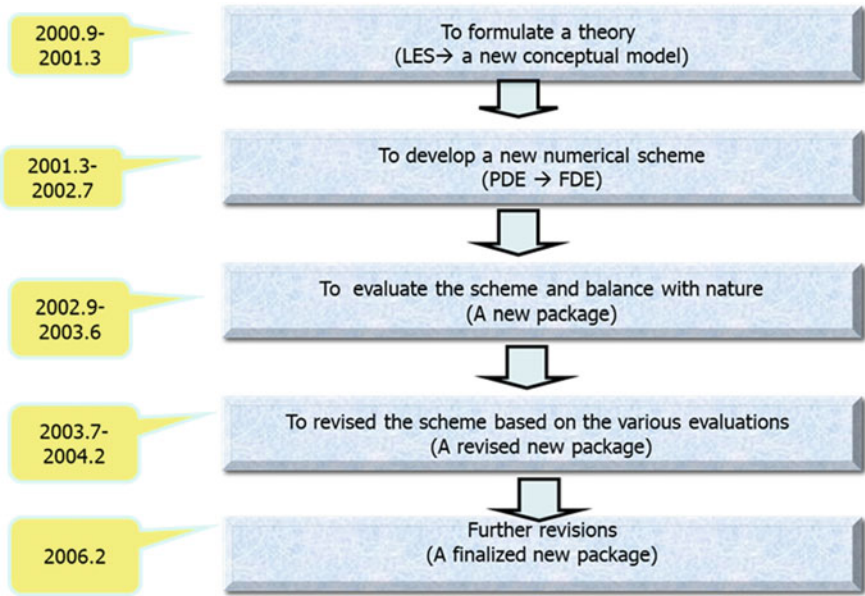


Fig. 5.6 Schematic of YSU PBL development

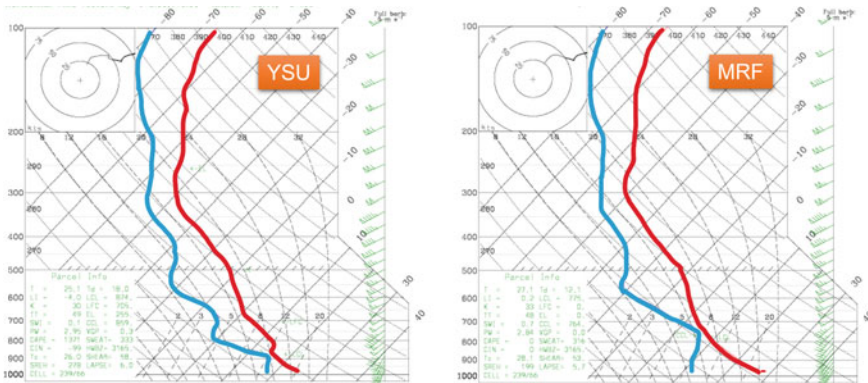


Fig. 5.7 Simulated sounding near Nashville, TN, obtained from the experiments with the YSU (left), MRF (middle) PBL, and the observed (right) at 1800 UTC 10 Nov 2002. The number on the lower left corner indicates the level of inversion layer, which is 870 mb, 865 mb, and 720 mb, respectively

experiments in the previous section. The MRF PBL is particularly active in this case because of a strong 20 m s^{-1} southwesterly flow just above the boundary layer. This leads to a decrease in the PBL’s Rib used to compute the boundary layer height, enhancing the entrainment above the inversion layer. In the YSU PBL scheme, the shear only contributes in a secondary way to enhance entrainment, which is governed

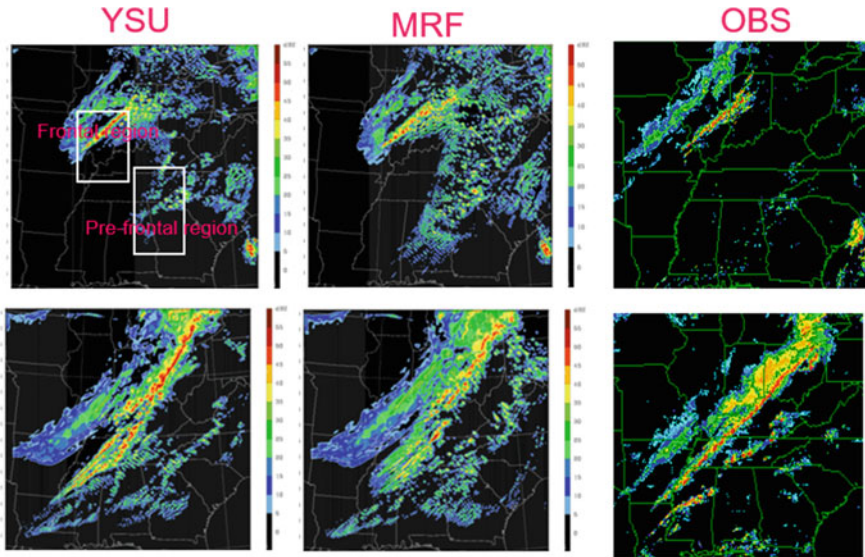


Fig. 5.8 Composite maximum reflectivity (dBZ) at 1800 UTC 10 November (upper) and 0000 UTC 11 November (lower) from the YSU (left) and MRF (middle) experiments and the corresponding observations (right)

mainly by the magnitude of the surface fluxes and thus does not maximize until later in the day. Despite the higher CAPE with the YSU PBL compared with the MRF PBL, the radar reflectivity showed the weakening of convection in the prefrontal region. Examining the frontal and prefrontal areas can better explain the reason. It is seen that the light precipitation in front of intense convection is better captured by the YSU PBL than the MRF PBL. In the area of intense convection, the model underestimated the precipitation amount irrespective of the choice of the PBL scheme. Still, the YSU PBL scheme better captured the time variation of the precipitation associated with late afternoon convection after 2100 UTC on 10 November 2002 (Fig. 5.8).

The different impacts can be attributed to the differences in the synoptic environment associated with the formation of convection. Upward motion prevails within the entire troposphere, and cloud tops reach the tropopause, whereas the downward motion is dominant above the PBL ahead of a front. Ice microphysics is the critical mechanism, whereas warm clouds are prevalent in the prefrontal region. This indicates that, in contrast to the prefrontal area, the PBL processes play a secondary role in the intense convection region. Because of the weakened mixing in the YSU PBL, the PBL clouds are weakened before 2100 UTC on 10 November, but with a negligible difference. Because the synoptic environment associated with frontal convection is strong, the difference in the PBL mixing does not influence the overall evolution of daytime convection. The enhanced convection in the late afternoon in the case of the YSU PBL is due to the moister boundary layer below clouds, which reduces the evaporation of falling precipitation. The resulting overall impact is that

the boundary layer from the YSU PBL scheme remains less diluted by entrainment, leaving more fuel for severe convection when the front triggers it (see Hong et al. (2006) for details).

In addition to the dependency of PBL processes on the synoptic environment concerning precipitating mechanisms, an essential lesson in Hong et al. (2006) is that PBL processes play a critical role not only in modulating convection triggering but also in providing PBL structure directly affecting cloud microphysical processes when they fall near the surface.

After the YSU scheme was officially announced to the WRF community in early 2000, some systematic biases were reported. One is an underestimate of the chemical species over cold-water bodies (Kim et al. 2008, WRF workshop). Another is underestimating PBL heights at nighttime (2006, F. Zhang, personal communication). He noticed that the nocturnal PBL heights in WRF using the YSU scheme are nearly constant between 0 and 20 m. Lidar data from the recent Mexico City field campaign reveal nocturnal PBL heights vary between 20 and 500 m, with strong winds corresponding to large PBL heights. Cold and wet biases were reported at nighttime in the real-time operation of WRF over East Asia at Seoul National University.

These systematic biases were regarded as due to insufficient mixing in the stable boundary layer, to which no attention was paid. The stable boundary layer was formulated as a local mixing in the MRF and YSU PBL schemes. Based on an observational analysis of stable boundary conditions (Vickers and Mahrt 2004), Hong (2010) formulated a new stable boundary-layer scheme by elevating the mixing height when winds are strong. The main idea is the same as in the Troen and Mahrt in the sense that h is determined by Rib_{cr} , which can be expressed as

$$Rib_{cr} = 0.16(10^{-7} R_o)^{-0.18}, \quad (5.22)$$

where $R_o = U_{10}/(fz_0)$ as in Vickers and Mahrt 2004. This formula is only valid when z_0 is a molecular roughness length over oceans. Over land, a theoretical value for turbulent activity ($= 0.25$) is employed.

Aside from the improvement of cold and wet biases by enhanced mixing in stable conditions, Hong (2010) demonstrated that the interaction of stable boundary layer and precipitation processes improves the summer monsoon precipitation climatology (Fig. 5.9). Compared to the CTL simulation results, the SBL experiment displaces the monsoonal rainfall southward, increasing rainfall amounts in Central China, Korea, and Japan. The results with the new SBL scheme demonstrate that modulating the subcloud structure with enhanced vertical mixing improves the simulated monsoon climatology by displacing the monsoonal precipitation southward. The behavior of northward displacement of simulated precipitation over East Asia in summer has been a systematic error in other regional climate models (Fu et al. 2005; Park et al. 2008). Some studies focused on the convective parameterization scheme to resolve this issue, but these biases remained unchanged irrespective of the selected scheme. Hong (2010) demonstrated that together with the local effects

of the enhanced SBL mixing that warms and dries the boundary layer, the dynamical feedback accompanying strengthened moisture convergence results in enhanced precipitation southward toward what was observed.

Hong (2010) further suggests that care should be taken in interpreting the results with the vertical diffusion package with some modifications since the boundary-layer structure significantly influences the simulated climate through interaction with other physical processes in weather and climate models, which is important for further improvement of existing schemes and developing a new parameterization method. Related to this issue, Kim and Hong (2009) confirmed that the new SBL scheme designed in this study plays a critical role in representing proper interaction between the BL and gravity-wave drag processes in a version of the NCEP global model, which leads to a significant improvement of seasonal climatology in terms of zonal wind and temperature.

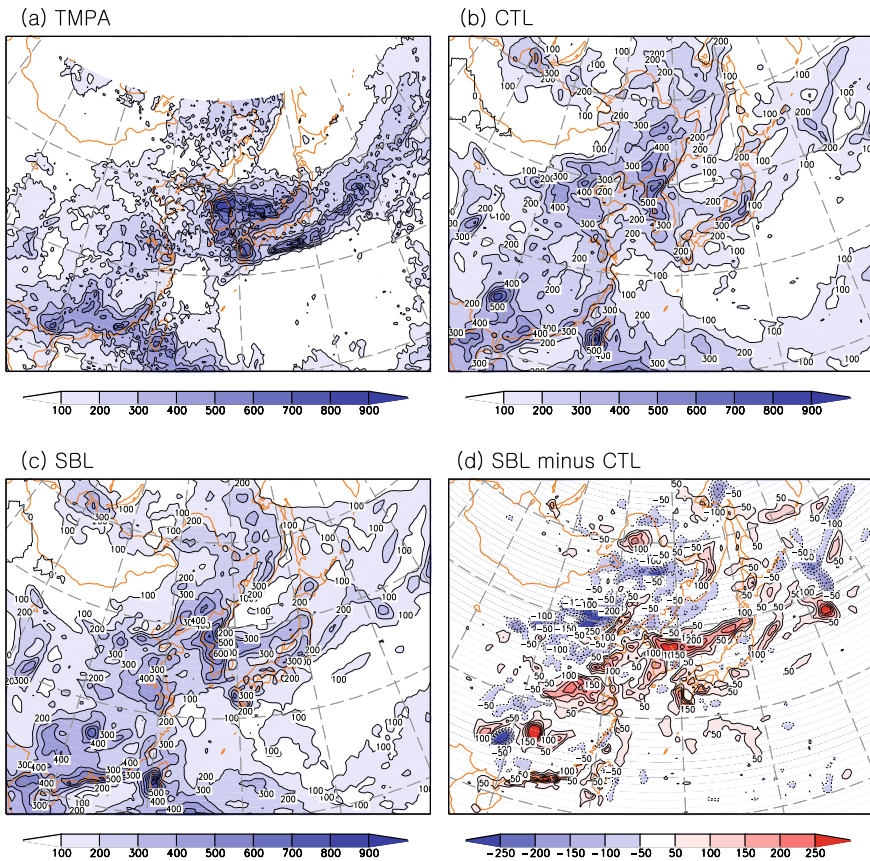


Fig. 5.9 Monthly accumulated precipitation (mm) for July 2006 from the, **a** TMPA observation, experiments with stable boundary-layer scheme in, **b** Hong et al. (2006) (CTL), **c** Hong (2010) (SBL), and **d** their differences

In 2010, too strong surface wind biases from the use of this scheme were reported by the WRF community. This behavior was found to be associated with the too strong nighttime mixing by this PBL scheme. In collaboration with Peggy LeMone at NCAR, the mixed layer velocity scale— $w_s = u_* \phi_m^{-1}$, Eq. (5.12)—was revised with $\phi_m = 1 + 5z/L$; with this revision, ϕ_m is computed as a function of z , whereas the original formulation of ϕ_m in Hong et al. (2006) is computed at a fixed height, i.e., the surface layer height at $z = z_l$ (lowest model level). By implementing the height dependency of ϕ_m into the scheme, the vertical mixing is reduced with height, alleviating the excessive nighttime mixing. Figure 5.10 demonstrates the temporal evolution of wind speed for the changes in WRF versions. WRF 3.2 is the same as in Hong (2010). WRF 3.4 with the revision in Pr , which affects the daytime mixing. WRF 3.4.1 reflects the above revision. The revised w_s enhances the nighttime LLJ by increasing the vertical gradient of wind speed. It is due to smaller eddy diffusivities in the nighttime boundary layer and, consequently, lower and stronger LLJs. As a result, related overestimation problems for near-surface temperature and wind speeds appear to be resolved, and the nighttime minimum near-surface O3 concentrations are better captured (Hu et al. 2013).

Various evaluation testbeds have been applied in developing/revising the YSU PBL scheme. First, a theoretical concept is derived based on evaluations of the WRF community and the scheme developer. In the case of YSU PBL, a new formula based on an updated LES is the core part (Noh et al. 2003). Numerical discretization considering the characteristics of NWP and climate models should be followed,

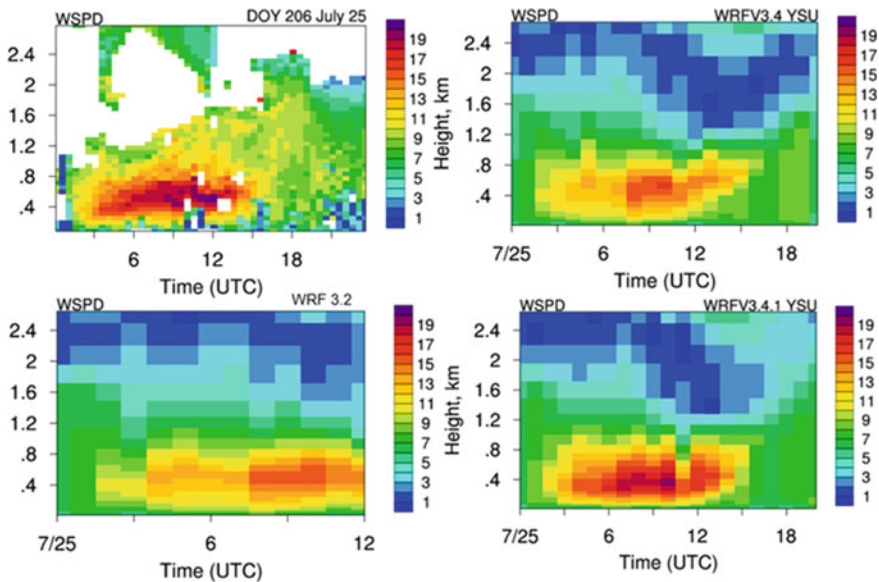


Fig. 5.10 Wind speed from observation (upper left) WRF version 3.2 (lower left), 3.4 (upper right), and 3.4.1 (lower right)

assuring that the discretized scheme coupled with simple physics in atmospheric models reproduces the same behavior in LES studies. Second, evaluate the revisions in full physics models. Since evaluation results are combined products between PBL and all other physical processes, care should be taken in interpreting results. Process study for each component of the revised scheme needs to be followed. Considering the interaction with other physical processes as in nature, refinement and/or reformulation should be followed. Finally, the revised scheme should positively impact the short-medium-long-range forecasts with the forecast skill score. For instance, WRF and other global and regional models, such as GRIMs, were utilized to evaluate the performance of the new scheme (e.g., Byun and Hong 2004). Another example is the interaction between the orography-induced gravity-wave drag and boundary-layer processes in a global atmospheric model (e.g., Kim and Hong 2009). They showed that stable boundary is limited in the lower troposphere, but it enables the significant modulation of planetary-scale waves in the stratosphere through the upward propagation of gravity waves that originated near the surface.

5.3.3 *Shin-Hong PBL Scheme*

In the summer of 2010, scientists from operational and research institutes in Korea, Japan, France, England, Finland, and the USA met to discuss recent developments in the parameterizations of physical processes for next-generation, high-resolution numerical weather prediction (NWP) models. The meeting summaries are provided by Hong and Dudhia (2012). The main topic of the workshop focused on future problems in physics parameterizations as NWP models go to finer horizontal model resolutions where there exist “gray zones” in which the explicit model dynamics is capable of partially resolving features that are entirely parameterized at coarser resolutions, e.g., deep and shallow moist convection, and turbulence in the PBL, particularly in the convective PBL (CBL). In the gray zone of an atmospheric process, model grid spacing (Δ) is comparable to the process’s characteristic scale (l) to be parameterized, i.e., $\Delta \sim l$. For example, the gray zone of the CBL and shallow cumulus convection is approximately 0.1–1 km (Honnert et al. 2011; Dorrestijn et al. 2013; Shin et al. 2013). The gray zone scale decreases to 10–100 m (Honnert et al. 2020) in the neutral ABL (NBL) as l decreases with the absence of buoyancy to generate thermally driven turbulence. It may be a decade before the NBL gray-zone issues must be addressed. Hereafter, discussions focus on the CBL gray zone.

One-dimensional (1D) PBL schemes are adequate at grid sizes above a few kilometers where no CBL turbulence eddies are resolved ($\Delta \gg l$). However, in the CBL “gray zone” ($\Delta \sim l$), new types of PBL parameterizations are needed to adjust the amount of parameterized SGS turbulence in response to the partially resolved turbulence. There was also discussion about extending the use of three-dimensional (3-D) SGS models in large-eddy simulation (LES) to the PBL gray zone (as used for many years in cloud-resolving models at grid spacings of 0.1–1 km). At LES grid sizes—for example, grid sizes of 100 m or smaller for the CBL—it is considered

that the model dynamics explicitly resolve nonlocal vertical transport by coherent and well-organized large eddies, i.e., ① on the rhs of Eq. (5.2). All SGS turbulence is assumed locally isotropic. All SGS mixing can be represented by 3D local mixing with LES SGS models. LES SGS turbulence models work well in the inertial subrange, but their assumptions break down in the gray zone. This challenge in numerical modeling of turbulence, where Δ and l are of the same order is well-documented in the pioneering study by Wyngaard (2004).

To develop a new SGS parameterization for the CBL gray zone, an investigation of how the characteristics of the SGS turbulence to be parameterized change with model grid spacing must take precedence. Honnert et al. (2011) (hereafter, HMC11) proposed an original method to quantify the amount of the SGS vertical turbulent fluxes and TKE, using LES results of different types of CBLs (i.e., free convection, shear- and buoyancy-driven, and cloud-topped CBLs). They applied a simple spatial filtering to the LES results for the spatial filter size (that represents Δ) ranging between their LES grid spacing (Δ_{LES}) and LES domain size (D).

Shin and Hong (2013) (hereafter, SH13) further extended the LES study of HMC11 by implementing the effects of CBL stability into the grid-size dependency functions. They computed the grid-size dependencies of SGS nonlocal and local vertical transports in CBLs at gray-zone resolutions, using a 25-m-resolution WRF-LES as the benchmark. They produced reference data for gray-zone grid spacing by spatially filtering the benchmark LES (Fig. 5.11). In their analysis, the amount of SGS vertical transport could be partitioned at each grid (Δ), along with the scale dependency of the total (nonlocal plus local) SGS transport. This is consistent with the key finding of Honnert et al. (2011), who revealed that the inclusion of the mass-flux term is more important than the formulation of eddy diffusivity in determining the grid-size dependency of the parameterized transport in the gray zone. SH13 further decomposed turbulent vertical mixing into two components—nonlocal mixing and local mixing—and examined the grid-size dependency functions of these two components separately. They found that the nonlocal mixing component is more sensitive to the CBL stability, and the amount of the nonlocal transport is larger than the local part. SH13 also demonstrated that the effects of CBL stability need to be considered in developing a new gray-zone CBL parameterization by implementing the stability effects into the nonlocal mixing term.

Based on the conceptual derivation by SH13, Shin and Hong (2015) (hereafter, SH15) proposed a new PBL parameterization that replaces the CBL mixing algorithm of the YSU PBL scheme with an LES-informed scale-adaptive vertical mixing algorithm. First, nonlocal transport by large eddies and local transport by remaining smaller eddies are separately parameterized. Second, the SGS nonlocal transport is newly formulated by replacing the countergradient and the explicit entrainment terms of the YSU PBL scheme with an LES-fitted nonlocal mixing profile. The nonlocal mixing profile is multiplied by a grid-size dependency function, and the impact of CBL stability is implemented into the grid-size-dependent function. Finally, the SGS local transport is formulated by multiplying a grid-size dependency function by the K-profile diffusivity of the YSU PBL scheme. This new scheme is called as Shin-Hong PBL scheme. SH15 demonstrated that the new scheme increases the resolved

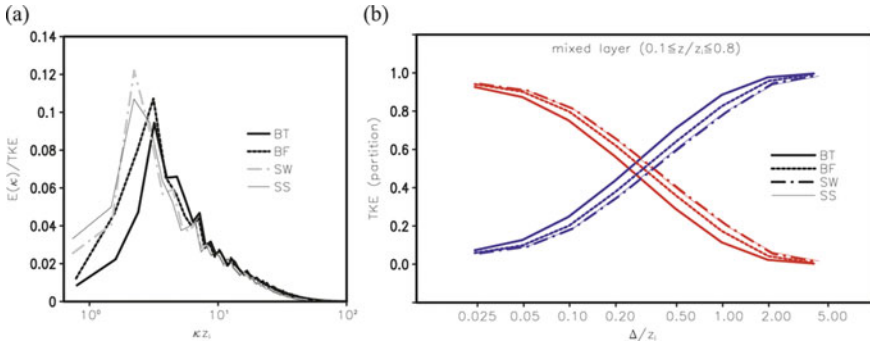


Fig. 5.11 **a** Two-dimensional energy spectra at $z/z_i = 0.5$, normalized by total TKE. **b** Ratio of resolved (red) and subgrid-scale (blue) TKE to total TKE as functions of dimensionless grid size (Δ/z_i): for cases BT (buoyancy-driven and organized thermals; thick solid), BF (buoyancy-driven and wind forced; thick dotted), SW (weak shear-driven; thick dotted-dashed), and SS (strong shear-driven; thin solid). From Shin and Hong (2013). ©American Meteorological Society. Used with permission

energy, which is toward the reference spectra in sub-kilometer resolutions. The new algorithm produces mean temperature profiles closer to the LES results than the YSU scheme. Between the two most significant modifications from the YSU PBL scheme (a change in the total nonlocal transport profile and inclusion of the scale dependency), the improvement in the mean profiles is mainly due to the revised total nonlocal transport profile fit to the LES data. The grid-size dependency functions help the resolved motions and resolved transport profiles improve via accurately computing the SGS transport profiles at different resolutions.

5.3.4 3D TKE-Based Scale-Aware Scheme (3D TKE, Zhang et al. 2018)

To address the requirement for the gray-zone issue, a scale-adaptive parameterization scheme of 3D turbulent mixing based on the whole 3D TKE prognostics equation has been developed to represent turbulent mixing on subgrid scales in the gray zone (Zhang et al. 2018). In this scheme, the TKE-based parameterization scheme for turbulent mixing commonly used for LES is revised to be suitable for resolutions typically used in a mesoscale model. In particular, this scheme provides a pathway to consider all the components of the Reynolds-stress tensor in a coherent, more general framework, making it feasible to replace conventional 1D PBL schemes with the scale-adaptive 3D TKE-based scheme.

In convective boundary layer (CBL), coherent structures due to the buoyancy dominate the vertical turbulent flux in a nonlocal way (Shin and Hong 2013; Hellsten and Zilitinkevich 2013). The flux productions can be expressed by conventional

eddy-diffusivity models including the nonlocal effects as follows:

$$\overline{u'_i u'_j} = -K_{ij}^M \left(\frac{\partial \bar{u}_i}{\partial x_j} + \frac{\partial \bar{u}_j}{\partial x_i} \right) + \delta_{i3} \overline{u'_i u'_j}^{\text{NL}}, \quad (5.23)$$

$$\overline{u'_i \theta'} = -K_{ij}^H \frac{\partial \bar{\theta}}{\partial x_j} + \delta_{i3} \overline{u'_i \theta'}^{\text{NL}}, \quad (5.24)$$

where superscripts M , H , and NL indicate momentum, heat, and nonlocal, respectively. That is, both subgrid-scale stress and heat flux can be decomposed into two components: the local flux due to the gradient of mean fields and the nonlocal flux due to the buoyant-production terms. Note that the nonlocal terms are only retained in the vertical because they are directly related to the buoyancy-driven transport.

A pragmatic approach based on Shin and Hong 2013 for the transition of vertical turbulent mixing across the gray zone is adopted in this scheme. That is, the heat flux for particular grid size Δ can be divided into the local and nonlocal components:

$$\overline{w' \theta'}^\Delta = -K_{Hv}^\Delta \frac{\partial \bar{\theta}}{\partial z} + \overline{w' \theta'}^{\Delta, \text{NL}} = \overline{w' \theta'}^{\Delta, L} + \overline{w' \theta'}^{\Delta, \text{NL}}, \quad (5.25)$$

where the superscript L and NL refer to local and nonlocal, respectively. The subscript v refers to vertical. The nonlocal flux term is multiplied by the partition function $P_{\text{NL}}(\Delta/z_i)$ shown in Fig. 5.11 as follows:

$$\overline{w' \theta'}^{\Delta, \text{NL}} = \overline{w' \theta'}^{\text{NL}} P_{\text{NL}}(\Delta/z_i), \quad (5.26)$$

where $\overline{w' \theta'}^{\text{NL}}$ the nonlocal heat flux at the mesoscale.

The vertical eddy diffusivity is formulated as $K_{Hv}^\Delta = L_\Delta e^{1/2}$ for Δ , the corresponding local heat flux is expressed as

$$\overline{w' \theta'}^{\Delta, L} = -K_{Hv}^\Delta \frac{\partial \bar{\theta}}{\partial z} = -L_\Delta e^{1/2} \frac{\partial \bar{\theta}}{\partial z}. \quad (5.27)$$

The length scale L_Δ is obtained by blending the LES length scale $L_{\text{LES}} = c_{k1} l_{\text{LES}}$ and the mesoscale length scale $L_{\text{Meso}} = c_{k2} l_{\text{Meso}}$ using the partition function $P_{\text{NL}}(\Delta/z_i)$, where $ck1$ and $ck2$ are dimensionless constants,

$$L_\Delta = P_{\text{NL}}(\Delta/z_i) L_{\text{Meso}} + [1 - P_{\text{NL}}(\Delta/z_i)] L_{\text{LES}}. \quad (5.28)$$

Note that the dimensionless constants c_{k1} and c_{k2} are different at LES and mesoscale limits. The transition of horizontal diffusion across the gray zone is introduced as follows:

$$K_h = P_{\text{NL}}(\Delta x/z_i) K_D + [1 - P_{\text{NL}}(\Delta x/z_i)] K_T, \quad (5.29)$$

where K_D is the horizontal diffusivity based on the deformation (i.e., Smagorinsky-type formula), K_T is the horizontal diffusivity based on the TKE. And c_s and c_k are dimensionless constants.

In the development of the scheme, specific attention was given to the determinations of nonlocal heat/momentum flux and the master mixing length for vertical mixing. A series of dry convective boundary layer (CBL) idealized simulations were also carried out by Zhang et al. (2018) to compare the scheme's performance with the conventional treatment of subgrid mixing using the ARW-WRF-LES dataset, highlighting the importance of including the nonlocal component for vertical turbulent mixing in this new scheme. The improvements of the new scheme over the conventional treatment of subgrid mixing across the gray zone were also in these idealized simulations. Results from real-case simulations also showed the feasibility of using this new scheme in a mesoscale model in place of the conventional treatment of turbulent mixing on subgrid scales.

As compared to the Shin-Hong scheme in the previous subsection, the new scheme is advanced since it bridges the numerical dissipation and turbulence properties explicitly via 3D TKE. The conventional approach such as YSU scheme underestimates the resolved kinetic energy when grid spacing is smaller than a few kilometers and deficiency becomes substantial at sub-kilometers (Fig. 5.12). Shin-Hong scheme represents the gray zone by empirical function that is derived from the filtered LES data. Thus, this scheme implicitly represents the isotropic turbulence at LES scales. Meanwhile, the 3D-TKE scheme (Zhang et al. (2018)) represents the transition from isotropic to anisotropic eddies using a predicted 3D TKE in an explicit manner. Both schemes commonly utilize the same nonlocal transport terms and a similar scale-aware functionality. Further research is required to elucidate the turbulent properties at LES or higher resolutions.

It should be noted that adequately representing horizontal turbulent mixing in the gray zone remains a research subject. Some horizontal turbulent mixing schemes are implemented in global and mesoscale models primarily for numerical purposes, e.g., to remove small-scale noise with wavelengths of 2–4 times the grid intervals (Xue 2000; Knierel et al. 2007; Langhans et al. 2012). Others are intended to mimic unresolved subgrid-scale mixing processes following Smagorinsky (1963). Recently, more and more studies addressed the importance of horizontal turbulent mixing in more realistic cases to evaluate and quantify horizontal turbulent mixing (Bryan and Rotunno 2009; Rotunno and Bryan 2012; Bryan 2012; Machado and Chaboureau 2015). Honnert (2016) calculated the horizontal mixing length from LES of neutral and convective cases in the gray zone resolutions.

5.4 Future Directions

In conclusion, there has been a general trend from very simple dry local mixing approaches in earlier models to ABL schemes that represent nonlocal transport by thermals, cloud effects, top-down mixing, etc., thus including the full spectrum of

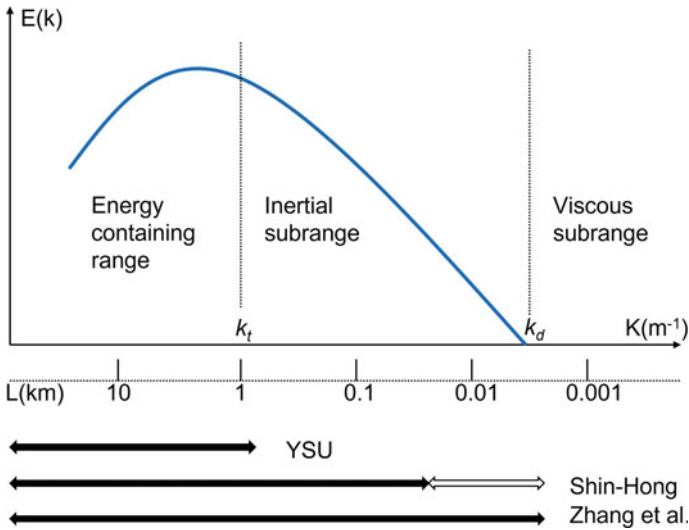


Fig. 5.12 A schematic of the turbulent kinetic energy spectra in the convective boundary layer. Its density is depicted as a function of wave number K and of the corresponding length scale $L = 2\pi/K$. k_t and k_d represent the turbulence length scale and dissipation scale, respectively. Thick lines with arrows indicate the scale for a specific scheme to be eligible explicitly. An open arrow in Shin-Hong scheme represents a range of implicit coupling with numerical dissipation

ABL types within a single parameterization scheme and enabling improvements in representing the evolution of low cloud cover. The idea that ABL schemes should be unified with shallow cumulus schemes has been gaining popularity with the concept of top-down radiatively driven mixing that influences boundary layer growth and shallow cloud development. There are further ambitious efforts to extend this to deep convection (e.g., Park 2014), but deep convection contains net diabatic and internal dynamical effects that are not representable by simple transport or reversible thermodynamics, and it is debatable whether this can be unified with the more reversible and mixing-like processes of shallow convection and PBL schemes.

As the resolution of NWP models approaches sub-kilometer scales, three-dimensional mixing becomes more relevant, and some new gray-zone approaches transition to fully three-dimensional large-eddy schemes that do not require nonlocal vertical mixing as boundary-layer eddies resolve by the dynamics. Consistent treatment of horizontal and vertical turbulent mixing is still one of the challenging problems in atmospheric model development for gray-zone resolution simulations. There is no converging theory for quantifying the intensity of horizontal mixing. Few observations are available to constrain the quantitative aspects of the parameterization (e.g., the horizontal mixing length). However, as an example, Hanley et al. (2015) investigated the sensitivity of the storm morphology and statistical properties to horizontal mixing. They evaluated it against rainfall measurements of a radar network. Nevertheless, since horizontal turbulent mixing is dynamically coupled with vertical

mixing across the gray zone, future development of vertical turbulent mixing parameterization on subgrid scales should consider the physical consistency between the vertical and horizontal mixing for atmospheric simulations at gray-zone resolutions.

Even as the convective boundary layer becomes better represented at higher resolutions, challenges remain with the stable boundary and complex environments (terrain, urban, forests) that will still require subgrid parameterizations using knowledge of heterogeneity with grid cells.

Acknowledgements The authors wish to acknowledge collaborations with Hua-Lu Pan, Yign Noh, Xu Zhang, Baode Chen, and Evelyn Grell. Comments on the manuscript from anonymous reviewers should be acknowledged.

References

- Beare RJ (2014) A length scale defining partially-resolved boundary-layer turbulence simulations. *Bound-Layer Meteorol* 151:39–55. <https://doi.org/10.1007/s10546-013-9881-3>
- Blackadar AK (1979) High resolution models of the planetary boundary layer. In: Pfafflin J, Ziegler E (eds) *Advances in environmental science and engineering*, vol 1, no 1. Gordon and Breach, pp 50–85
- Bretherton CS, Park S (2009) A new moist turbulence parameterization in the community atmosphere model. *J Clim* 22:3422–3448. <https://doi.org/10.1175/2008JCLI2556.1>
- Bryan GH (2012) Effects of surface exchange coefficients and turbulence length scales on the intensity and structure of numerically simulated hurricanes. *Mon Weather Rev* 140:1125–1143. <https://doi.org/10.1175/MWR-D-11-00231.1>
- Bryan GH, Rotunno R (2009) The maximum intensity of tropical cyclones in axisymmetric numerical model simulations. *Mon Weather Rev* 137:1770–1789. <https://doi.org/10.1175/2008MWR2709.1>
- Byun YH, Hong SY (2004) Impact of boundary-layer processes on simulated tropical rainfall. *J Clim* 17:4032–4044. [https://doi.org/10.1175/1520-0442\(2004\)017%3C4032:IOBLPO%3E2.0.CO;2](https://doi.org/10.1175/1520-0442(2004)017%3C4032:IOBLPO%3E2.0.CO;2)
- Deardorff JW (1972) Parameterization of the planetary boundary layer for use in general circulation models. *Mon Weather Rev* 100:93–106. [https://doi.org/10.1175/1520-0493\(1972\)100%3C0093:POTPBL%3E2.3.CO;2](https://doi.org/10.1175/1520-0493(1972)100%3C0093:POTPBL%3E2.3.CO;2)
- Dorrestijn JD, Crommelin T, Siebesma AP et al (2013) Stochastic parameterization of shallow cumulus convection estimated from high-resolution model data. *Theor Comput Fluid Dyn* 27:133–148. <https://doi.org/10.1007/s00162-012-0281-y>
- Fu FB, Wang S, Xiong Z et al (2005) Regional climate model intercomparison project for Asia. *Bull Am Meteorol Soc* 86:257–266. <https://doi.org/10.1175/BAMS-86-2-257>
- Han J, Witek ML, Teixeira J et al (2016) Implementation in the NCEP GFS of a hybrid eddy-diffusivity mass-flux (EDMF) boundary layer parameterization with dissipative heating and modified stable boundary layer mixing. *Weather Forecast* 31:341–352. <https://doi.org/10.1175/WAF-D-15-0053.1>
- Hanley KE, Plant RS, Stein THM et al (2015) Mixing-length controls on high-resolution simulations of convective storms. *Q J R Meteorol Soc* 142:272–284. <https://doi.org/10.1002/qj.2356>
- Hellsten A, Zilitinkevich S (2013) Role of convective structures and background turbulence in the dry convective boundary layer. *Bound-Layer Meteorol* 149:323–353. <https://doi.org/10.1007/s10546-013-9854-6>

- Holtstlag AAM, Boville BA (1993) Local versus nonlocal boundary-layer diffusion in a global climate model. *J Clim* 6:1825–1842. [https://doi.org/10.1175/1520-0442\(1993\)006%3C1825:LVNBLD%3E2.0.CO;2](https://doi.org/10.1175/1520-0442(1993)006%3C1825:LVNBLD%3E2.0.CO;2)
- Hong SY (2010) A new stable boundary-layer mixing scheme and its impact on the simulated East Asian summer monsoon. *Q J R Meteorol Soc* 136:1481–1496. <https://doi.org/10.1002/qj.665>
- Hong SY, Pan HL (1996) Nonlocal boundary layer vertical diffusion in a medium-range forecast model. *Mon Weather Rev* 124:2322–2339. [https://doi.org/10.1175/1520-0493\(1996\)124%3C2322:NBLVDI%3E2.0.CO;2](https://doi.org/10.1175/1520-0493(1996)124%3C2322:NBLVDI%3E2.0.CO;2)
- Hong SY, Noh Y, Dudhia J (2006) A new vertical diffusion package with an explicit treatment of entrainment processes. *Mon Weather Rev* 134:2318–2341. <https://doi.org/10.1175/MWR3199.1>
- Hong SY, Dudhia J (2012) Next-generation numerical weather prediction: bridging parameterization, explicit clouds, and large eddies. *Bull Am Meteorol Soc* 93:ES6–ES9. <https://doi.org/10.1175/2011BAMS3224.1>
- Honnert R (2016) Representation of the grey zone of turbulence in the atmospheric boundary layer. *Adv Sci Res* 13:63–67. <https://doi.org/10.5194/asr-13-63-2016>
- Honnert R, Masson V, Couvreur F (2011) A diagnostic for evaluating the representation of turbulence in atmospheric models at the kilometric scale. *J Atmos Sci* 68:3112–3131. <https://doi.org/10.1175/JAS-D-11-061.1>
- Honnert R, Couvreur F, Masson V et al (2016) Sampling the structure of convective turbulence and implications for grey-zone parameterizations. *Bound-Layer Meteorol* 160:133–156. <https://link.springer.com/article/https://doi.org/10.1007/s10546-016-0130-4>
- Honnert R, Efstathiou GA, Beare RJ et al (2020) The atmospheric boundary layer and the “Gray Zone” of turbulence: a critical review. *J Geophys Res Atmos* 125. <https://doi.org/10.1029/2019JD030317>
- Hu XM, Klein PM, Xue M (2013) Evaluation of the updated YSU planetary boundary layer scheme within WRF for wind resource and air quality assessments. *J Geophys Res* 118:10490–10505. <https://doi.org/10.1002/jgrd.50823>
- Janjić ZI (1990) The step-mountain coordinate: physical package. *Mon Weather Rev* 118:1429–1443. [https://doi.org/10.1175/1520-0493\(1990\)118%3C1429:TSMCPP%3E2.0.CO;2](https://doi.org/10.1175/1520-0493(1990)118%3C1429:TSMCPP%3E2.0.CO;2)
- Kim SW, McKeen S, Frost G et al (2008) The sensitivity of ozone and its precursors to PBL transport parameterizations within the WRF-Chem model. In: *Proceedings of 7th WRF users’ workshop*, Boulder, Colorado, 19–22 June
- Kim YJ, Hong SY (2009) Interaction between the orography-induced gravity wave drag and boundary layer processes in a global atmospheric model. *Geophys Res Lett* 36:L12809. <https://doi.org/10.1029/2008GL037146>
- Knievel JC, Bryan GH, Hacker JP (2007) Explicit numerical diffusion in the WRF model. *Mon Weather Rev* 135:3808–3824. <https://doi.org/10.1175/2007MWR2100.1>
- Langhans W, Schmidli J, Schär C (2012) Mesoscale impacts of explicit numerical diffusion in a convection-permitting model. *Mon Weather Rev* 140:226–244. <https://doi.org/10.1175/2011MWR3650.1>
- LeMone MA, Angevine WM, Bretherton CS et al (2020) 100 years of progress in boundary layer meteorology. *Meteorol Monogr* 59:9.1–9.85. <https://doi.org/10.1175/AMSMONOGRAPHS-D-18-0013.1>
- Louis JF (1979) A parametric model of vertical eddy fluxes in the atmosphere. *Bound-Layer Meteorol* 17:187–202. <https://doi.org/10.1007/BF00117978>
- Machado LA, Chaboureaud JP (2015) Effect of turbulence parameterization on assessment of cloud organization. *Mon Weather Rev* 143:3246–3262. <https://doi.org/10.1175/MWR-D-14-00393.1>
- Mellor GL, Yamada T (1974) A hierarchy of turbulence closure models for planetary boundary layers. *J Atmos Sci* 31:1791–1806. [https://doi.org/10.1175/1520-0469\(1974\)031%3C1791:AHOTCM%3E2.0.CO;2](https://doi.org/10.1175/1520-0469(1974)031%3C1791:AHOTCM%3E2.0.CO;2)
- Mellor GL, Yamada T (1982) Development of a turbulence closure model for geophysical fluid problems. *Rev Geophys* 20:851–875. <https://doi.org/10.1029/RG020i004p00851>

- Nakanishi M, Niino H (2006) An improved Mellor-Yamada level 3 model: its numerical stability and application to a regional prediction of advecting fog. *Bound-Layer Meteorol* 119:397–407. <https://doi.org/10.1007/s10546-005-9030-8>
- Noh Y, Cheon WG, Hong SY et al (2003) Improvement of the K-profile model for the planetary boundary layer based on large-eddy simulation data. *Bound-Layer Meteorol* 107:401–427. <https://doi.org/10.1023/A:1022146015946>
- O'Brien JJ (1970) A note on the vertical structure of the eddy exchange coefficient. *J Atmos Sci* 27:1213–1215. [https://doi.org/10.1175/1520-0469\(1970\)027%3C1213:ANOTVS%3E2.0.CO;2](https://doi.org/10.1175/1520-0469(1970)027%3C1213:ANOTVS%3E2.0.CO;2)
- Olson JB, Kenyon JS, Angevine WA et al (2019) A description of the MYNN-EDMF scheme and the coupling to other components in WRF–ARW. In: NOAA technical memorandum OAR GSD-61, p 37. <https://doi.org/10.25923/n9wm-be49>
- Park S (2014) A unified convection scheme (UNICON). Part I: formulation. *J Atmos Sci* 71:3902–3930. <https://doi.org/10.1175/JAS-D-13-0233.1>
- Park S, Bretherton CS (2009) The University of Washington shallow convection and moist turbulence schemes and their impact on climate simulations with the community atmosphere model. *J Clim* 22:3449–3469. <https://doi.org/10.1175/2008JCLI2557.1>
- Park EH, Hong SY, Kang HS (2008) Characteristics of an East-Asian summer monsoon climatology simulated by the RegCM3. *Meteorol Atmos Phys* 100:139–158. <https://doi.org/10.1007/s00703-008-0300-0>
- Plaim JE (2007) A combined local and nonlocal closure model for the atmospheric boundary layer. Part I: model description and testing. *J Appl Meteorol Clim* 46:1383–1395. <https://doi.org/10.1175/JAM2539.1>
- Rotunno R, Bryan GH (2012) Effects of parameterized diffusion on simulated hurricanes. *J Atmos Sci* 69:2284–2299. <https://doi.org/10.1175/JAS-D-11-0204.1>
- Shin HH, Dudhia J (2016) Evaluation of PBL parameterizations in WRF at subkilometer grid spacings: turbulence statistics in the dry convective boundary layer. *Mon Weather Rev* 144:1161–1177. <https://doi.org/10.1175/MWR-D-15-0208.1>
- Shin HH, Hong SY (2013) Analysis of resolved and parameterized vertical transports in convective boundary layers at gray-zone resolutions. *J Atmos Sci* 70:3248–3261. <https://doi.org/10.1175/JAS-D-12-0290.1>
- Shin HH, Hong SY (2015) Representation of the subgrid-scale turbulent transport in convective boundary layers at gray-zone resolutions. *Mon Weather Rev* 143:250–271. <https://doi.org/10.1175/MWR-D-14-00116.1>
- Shin HH, Hong SY, Dudhia J (2012) Impacts of the lowest model level height on the performance of planetary boundary layer parameterizations. *Mon Weather Rev* 140:664–682. <https://doi.org/10.1175/MWR-D-11-00027.1>
- Siebesma AP, Soares PMM, Teixeira J (2007) A combined eddy-diffusivity mass-flux approach for the convective boundary layer. *J Atmos Sci* 64:1230–1248. <https://doi.org/10.1175/JAS3888.1>
- Smagorinsky J (1963) General circulation experiments with the primitive equations: I. The basic experiment. *Mon Weather Rev* 91:99–164. [https://doi.org/10.1175/1520-0493\(1963\)091%3C0099:GCEWTP%3E2.3.CO;2](https://doi.org/10.1175/1520-0493(1963)091%3C0099:GCEWTP%3E2.3.CO;2)
- Soares PMM, Miranda PMA, Siebesma AP et al (2004) An eddy-diffusivity/mass-flux parameterization for dry and shallow cumulus convection. *Q J R Meteorol Soc* 130:3365–3384. <https://doi.org/10.1256/qj.03.223>
- Stensrud D (2007) Parameterization schemes: keys to understanding numerical weather prediction models. Cambridge University Press, Cambridge. <https://doi.org/10.1017/CBO9780511812590>
- Stull RB (1988) An introduction to boundary layer meteorology. Kluwer Academic Publishers, Dordrecht, p 666
- Troen I, Mahrt L (1986) A simple model of the atmospheric boundary layer; sensitivity to surface evaporation. *Bound-Layer Meteorol* 37:129–148. <https://doi.org/10.1007/BF00122760>
- Vickers D, Mahrt L (2004) Evaluating formulations of stable boundary layer height. *J Appl Meteorol* 43:1736–1749. <https://doi.org/10.1175/JAM2160.1>

- Wilson TH, Fovell RG (2018) Modeling the evolution and life cycle of radiative cold pools and fog. *Weather Forecast* 33:203–220. <https://doi.org/10.1175/WAF-D-17-0109.1>
- Wyngaard JC (2004) Toward numerical modeling in the “Terra Incognita.” *J Atmos Sci* 61:1816–1826. [https://doi.org/10.1175/1520-0469\(2004\)061%3C1816:TNMITT%3E2.0.CO;2](https://doi.org/10.1175/1520-0469(2004)061%3C1816:TNMITT%3E2.0.CO;2)
- Xue M (2000) High-order monotonic numerical diffusion and smoothing. *Mon Weather Rev* 128:2853–2864. [https://doi.org/10.1175/1520-0493\(2000\)128%3C2853:HOMNDA%3E2.0.CO;2](https://doi.org/10.1175/1520-0493(2000)128%3C2853:HOMNDA%3E2.0.CO;2)
- Zhang DL, Anthes RA (1982) A high-resolution model of the planetary boundary layer—sensitivity tests and comparisons with SESAME-79 data. *J Appl Meteorol* 21:1594–1609. [https://doi.org/10.1175/1520-0450\(1982\)021%3C1594:AHRMOT%3E2.0.CO;2](https://doi.org/10.1175/1520-0450(1982)021%3C1594:AHRMOT%3E2.0.CO;2)
- Zhang X, Bao JW, Chen B et al (2018) A three-dimensional scale-adaptive turbulent kinetic energy scheme in the WRF-ARW model. *Mon Weather Rev* 146:2023–2045. <https://doi.org/10.1175/MWR-D-17-0356.1>
- Zhou B, Zhu K, Xue M (2017) A physically based horizontal subgrid-scale turbulent mixing parameterization for the convective boundary layer. *J Atmos Sci* 74:2657–2674. <https://doi.org/10.1175/JAS-D-16-0324.1>
- Zhou B, Sun S, Yao K et al (2018) Reexamining the gradient and countergradient representation of the local and nonlocal heat fluxes in the convective boundary layer. *J Atmos Sci* 75:2317–2336. <https://doi.org/10.1175/JAS-D-17-0198.1>